Computers and Mathematics with Applications 59 (2010) 2305–2314

Contents lists available at ScienceDirect

Computers and Mathematics with Applications

journal homepage: www.elsevier.com/locate/camwa

Lattice-Boltzmann studies of fluid flow in porous media with realistic rock geometries

Edo S. Boek*[,1], Maddalena Venturoli

Schlumberger Cambridge Research, High Cross, Madingley Road, Cambridge CB3 0EL, UK

ARTICLE INFO

Keywords:
Lattice Boltzmann
Porous media
Micromodel
X-ray microtomography

ABSTRACT

We present results of lattice-Boltzmann simulations to calculate flow in realistic porous media. Two examples are given for lattice-Boltzmann simulations in two- and three-dimensional (2D and 3D) rock samples. First, we show lattice-Boltzmann simulation results of the flow in quasi-two-dimensional micromodels. The third dimension was taken into account using an effective viscous drag force. In this case, we consider a 2D micromodel of Berea sandstone. We calculate the flow field and permeability of the micromodel and find excellent agreement with Microparticle Image Velocimetry (μ-PIV) experiments. Then, we use a particle tracking algorithm to calculate the dispersion of tracer particles in the Berea geometry, using the lattice-Boltzmann flow field.

Second, we use lattice-Boltzmann simulations to calculate the flow in Bentheimer sandstone. The data set used in this study was obtained using X-ray microtomography (XMT). First, we consider a single phase flow. We systematically study the effect of system size and validate Darcy's law from the linear dependence of the flux on the body force exerted. We observe that the values of the permeability measurements as a function of porosity tend to concentrate in a narrower region of the porosity, as the system size of the computational sub-sample increases. Finally, we compute relative permeabilities for binary immiscible fluids in the XMT rock sample.

1. Lattice-Boltzmann simulation of flow in 2D porous media

A fundamental understanding of flow in porous media is of crucial importance in many applications, such as the recovery of hydrocarbons from oil reservoirs. To characterise flow at the pore scale, it is convenient to use simplified representations of porous media, such as physical micromodels, which can be constructed in the form of pseudo-two-dimensional (pseudo-2D) capillary networks. Because the experimental analysis is often very difficult, simulation can be a useful complementary method. In particular, the lattice-Boltzmann technique is very well suited for solving the flow in complex geometries, and it has been successfully used in the study of flow in porous media at the pore scale [1–3]. For a general introduction to the lattice-Boltzmann theory, we refer to [4]. In two dimensions, lattice-Boltzmann simulations have been used to investigate viscous fingering of binary immiscible fluids using the Shan–Chen model [5] and the flow of non-Newtonian fluids in porous media [6,7]. In studies of viscous fingering in a Hele-Shaw cell, the third dimension was taken into account using an effective viscous drag force [8,9]. Recently, we used the effective viscous drag method to compare lattice-Boltzmann simulations of a single phase flow in micromodels with experimental results in the same geometry [10]. Here, we extend these calculations to flow in a 2D micromodel of Berea sandstone. We calculate the permeability of the micromodel and

* Corresponding author.
E-mail addresses: esb30@cam.ac.uk, e.boek@imperial.ac.uk (E.S. Boek), mventuro@cims.nyu.edu (M. Venturoli).
[1] Current address: Department of Chemical Engineering, Imperial College London, SW7 2AZ, UK.

0898-1221/$ – see front matter © 2009 Elsevier Ltd. All rights reserved.
doi:10.1016/j.camwa.2009.08.063

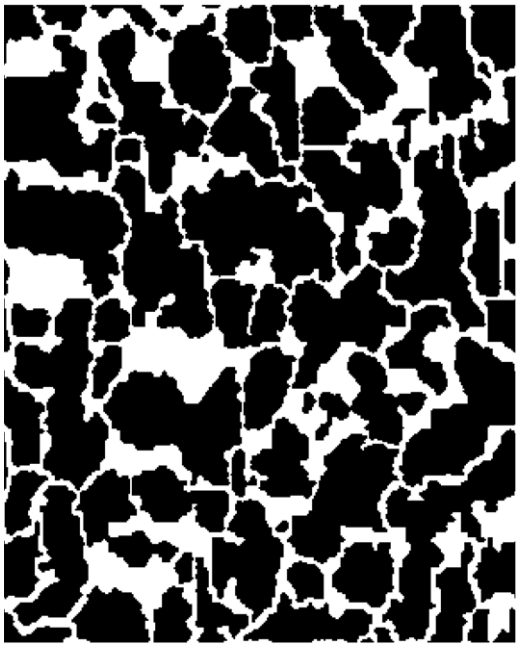

Fig. 1. Berea pattern used in the lattice-Boltzmann 2D simulations. The obstacles are represented in black, and the pore space in white. The size is 1418 μm by 1774 μm. The etch depth of the physical Berea unit is 24.54 μm.

compare with experimental data. Then, we use a particle tracking algorithm to calculate the dispersion of tracer particles in the Berea geometry, using the lattice-Boltzmann velocity field.

1.1. Berea sandstone

We study the flow in a 2D micromodel of Berea sandstone. This micromodel has been engineered at Schlumberger Cambridge Research, based on a thin section of a 3D Berea sandstone rock sample. The micromodel has been discretised on a lattice, and bit-mapped (0 pore, 1 obstacle) to create the matrix for the lattice-Boltzmann simulations. A picture of the Berea micromodel is presented in Fig. 1.

1.1.1. Single phase flow

We consider the lattice-Boltzmann method for flow in two dimensions, which has been described in detail in [10]. In that work, we have shown that we can make successful use of the Hele-Shaw viscous drag approximation when the third dimension of the micromodel is small in comparison with the lateral two dimensions. The micromodel described here is pseudo-2D, and, for symmetry reasons, the fluid velocity is zero in the z direction (depth). We adopt an approach used in the literature [11,8] to solve the flow field in such a geometry using 2D lattice-Boltzmann simulations. This approach consists in introducing a drag force, acting on the fluid, that represents the (approximate) effect of the bounding walls in the third dimension. This viscous drag force depends on the fluid kinematic viscosity, ν, on the fluid velocity, $\mathbf{u}$, and on a depth parameter, h, which represents the distance between the walls bounding the implicit third dimension. If the average velocity of the Poiseuille profile is used, the drag force takes the expression used by Boon et al. [8,9]

$$\mathbf{f}_{\text{drag}} = -\frac{12\nu}{h^2}\mathbf{u}. \tag{1}$$

This is the expression that we will use here.

1.1.2. Calculation of permeability

The permeability of a porous medium can be calculated from the empirical Darcy's law. This well known relation states that the flow rate is proportional to the force driving the fluid, the coefficient of proportionality being the permeability of the medium divided by the dynamic viscosity of the fluid. Darcy's law can be written as

$$J = -\frac{K}{\mu}(\nabla P - \rho g), \tag{2}$$

where J is the flow rate per unit area of cross section (flux), K is the permeability, ∇P is the pressure drop between inlet and outlet, ρ is the fluid density, g is a body force (for example gravity), and μ is the dynamic viscosity of the fluid (with the

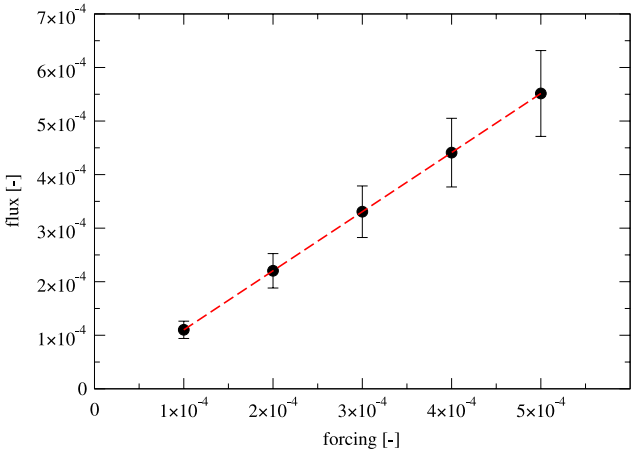

Fig. 2. Flux versus force and linear fit (dashed line) of the data points.

kinematic viscosity given by $\nu = \mu/\rho$). By measuring (or calculating) the flux for different pressure drops (or body force values), and using Eq. (2), the permeability K can be derived. The permeability has dimensions of an area, and it is measured in units of Darcy.

1.1.3. Single phase permeability

We have carried out lattice-Boltzmann simulations to calculate the single phase permeability of the micromodel using Darcy's law. To estimate the single phase permeability of the sample, we impose a flow in the positive y direction of the rock. The flow is driven only by a body force g (and no pressure drop is explicitly present). A correspondence between the body force, g, and the pressure drop, ∇P, can be defined using the following equation,

$$\nabla P = \frac{(P_i - P_o)}{L} = g\rho \tag{3}$$

where P_i and P_o are the pressures at the inlet and outlet respectively, L is the distance between inlet and outlet, and ρ is the fluid density. Eq. (3) can be used to compare the simulations with experiments, in which usually a pressure drop is used to drive the fluid flow.

The precise form of the forcing term used, generalised for a multi-component fluid system, is specified as follows:

$$F^{\sigma} = g\, m^{\sigma} \sum_i \rho^{\sigma}(\mathbf{x} + \mathbf{c}_i)\mathbf{c}_i \tag{4}$$

where m^{σ} is the mass of the fluid component σ, and ρ^{σ} is the density of that component. We have taken $m^{red} = m^{blue} = 1$.

The dependence of permeability on the Hele-Shaw depth h was investigated, and we performed simulations at 5 different values of the body force for each value of h. Fig. 2 shows an example of a typical force–flux plot. We found that the best agreement with the experimental value of $K = 445 \pm 35$ mD is obtained for a Hele-Shaw depth $h = 20$ [l.u.]. At a lattice resolution $\delta x = 1.16$ μm, this corresponds to an actual depth of 23.2 μm, in excellent agreement with the experimentally observed etch depth of 24.54 μm. The full details of these calculations will be given in a forthcoming paper [12].

1.1.4. Single phase flow field

In this section we present the single phase flow field and compare with experiments available. In Fig. 3, we show a direct comparison between the steady state flow field in a Berea micromodel measured from PIV experiments [13] and lattice-Boltzmann simulations ($\delta x = 1.16$ μm and $h = 20$). We observe that the experimental and computational flow field are in qualitative agreement, in the sense that we identify the same regions of high flow rate in both experiment and simulation. A similar degree of qualitative agreement was found by Zerai et al. [14] for a simpler pore geometry where they studied velocity fields in a network model using both PIV experiments and CFD calculations.

1.2. Tracer dispersion

Here we describe a method to calculate the dispersion of tracer particles in the flow field computed from 2D lattice-Boltzmann simulations, as described in the previous section. These results can, in principle, be compared directly with micromodel experiments of colloid dispersion [15,16]. The probability distributions of tracer displacement, or displacement propagators, from the simulations can be compared with NMR propagators [17,18].

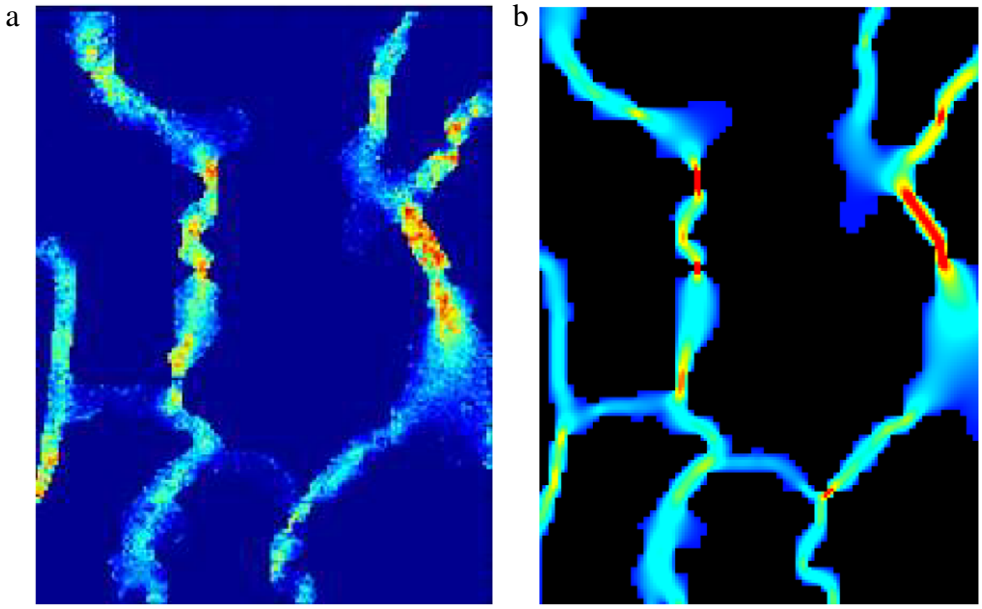

Fig. 3. Details of the flow field in a Berea micromodel measured from (a) PIV experiments [13] and (b) lattice-Boltzmann simulation of a computational cell with lateral resolution $\delta x = 2.32$ μm and Hele-Shaw depth $h = 10$. The colour coding runs from blue for low to red for high flow rates. (For interpretation of the references to colour in this figure legend, the reader is referred to the web version of this article.)

Following Maier et al. [19], in their study of dispersion in sphere packings, lattice-Boltzmann and Langevin equations can be used to model solvent flow and solute transport, respectively. The random walk of a tracer particle in an external velocity field is modeled by a stochastic differential equation for the particle position

$$\mathrm{d}\mathbf{x}(t) = \mathbf{v}(\mathbf{x}(t))\mathrm{d}t + \sqrt{2d\mathrm{D}_\mathrm{m}}\,\mathrm{d}W(t), \tag{5}$$

where d is the dimensionality of the system, $\mathbf{v}(\mathbf{x})$ is the fluid velocity computed from the lattice-Boltzmann simulations, D_m is the molecular diffusion ($\mathrm{D}_\mathrm{m} = 2.2 \times 10^{-9}$ m^2/s for water) and $\mathrm{d}W(t)$ is a Wiener process (Brownian motion). Eq. (5) can be solved using the forward Euler scheme

$$\mathbf{x}(t + \Delta t) = \mathbf{x}(t) + \mathbf{v}(\mathbf{x}(t))\Delta t + \sqrt{2d\mathrm{D}_\mathrm{m}\Delta t}\,\boldsymbol{\xi}, \tag{6}$$

where $\boldsymbol{\xi}$ is a unit vector whose orientation has a Gaussian distribution with zero mean and unit variance. For a more detailed description of the tracer dispersion algorithm, we refer to [12].

We use the velocity field obtained from the lattice-Boltzmann simulations described in the previous section. Then tracer particles are immersed in this velocity field and their evolution in time is computed using Eq. (6). The velocity field obtained using the value $h = 20$ (which gave the best results for the permeability calculations discussed above) is shown in Fig. 4(a). The tracer particles are initialised randomly in the pore space of the micromodel. In Fig. 4(b) the trajectory of a single tracer particle in this velocity field is shown. Note that periodic boundary conditions are applied. However, the displacement propagators are calculated using the total displacement. Typically, we used 10^4 to 10^5 tracer particles to obtain good statistics.

In Fig. 5 we show the tracer dispersion distributions for different observation times. The dispersion (or propagator) is the probability distribution of the tracer particle displacement (final position minus initial position) after a given amount of time. The shape of the propagators should be exponential at short time, with a peak at zero displacement (stagnant peak). The reason is that, for short observation times, the particles move within one pore. The distributions should become Gaussian for longer times, as the particles start to travel longer distances and to sample more pores. Our results in Fig. 5 show the exponential behaviour at short times, and a broadening of the profile as the observation time increases. However, even after 2000 ms, when a fully Gaussian profile is expected, the stagnant peak is still observed. This might be due to the fact that a 2D system has less connectivity than a 3D one, hence the particles trapped in stagnant zones are less likely to diffuse into zones with a non-zero velocity. This is a hypothesis that should be validated using micromodel experiments.

2. Lattice-Boltzmann simulation of flow in 3D porous media

In this section, we report on the calculation of the flow in a realistic complex 3D porous medium, in this case Bentheimer sandstone. In particular we study the dependence of the permeability measurement on the size of the computational sub-sample. With increasing sub-sample size, we find that the values of the permeability as a function of porosity tend to concentrate in a narrower region of the porosity. Finally, we calculate relative permeability curves for the case of immiscible flow.

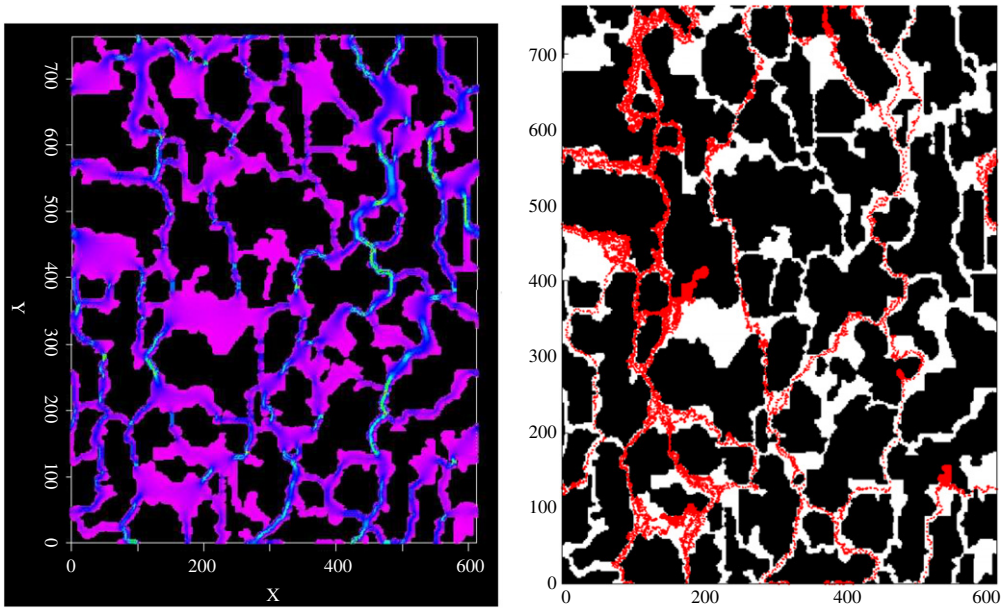

(a) Lattice-Boltzmann velocity field. (b) Tracer trajectory.

Fig. 4. (a) Velocity field in a 2D slice of Berea sandstone. The rock is shown in black and the velocity colour coding goes from zero velocity (pink) to increasing velocity (blue) to maximum velocity (green). Note that the colour coding is different from Fig. 3. Periodic boundary conditions are used in both dimensions. (b) Trajectory of a tracer particle (in red) with Brownian motion in the velocity field is shown in panel (a). (For interpretation of the references to colour in this figure legend, the reader is referred to the web version of this article.)

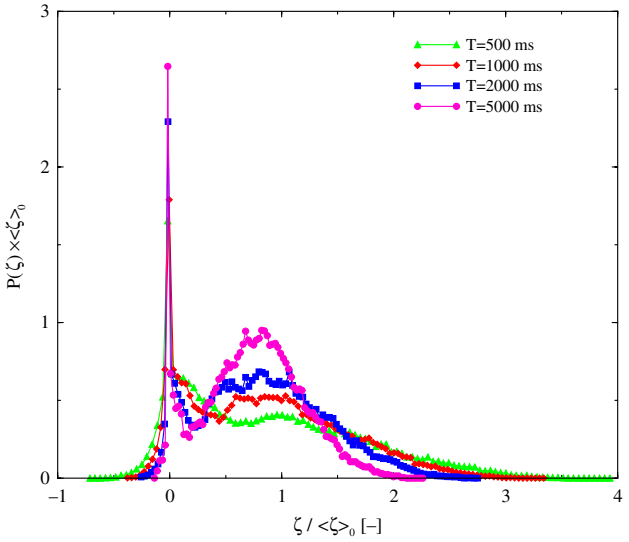

Fig. 5. Tracer dispersion propagators in the direction of the fluid flow (y-axis), for different observation times T and normalised with respect to the displacement $\langle\zeta\rangle_0$.

2.1. Materials and methods

2.1.1. Bentheimer sandstone

The data sets used in this study were extracted from the image of a cylindrical core of Bentheimer sandstone obtained by X-ray microtomography (XMT) at the European Synchrotron Research facility in Grenoble. The XMT image consists of voxels arranged in a 3D lattice. The full data set consists of approximately $800 \times 800 \times 630$ voxels, at a resolution of $\delta x = 4.9\ \mu$m. A 3D volume rendering of the data set is shown in Fig. 6. In the image data, each voxel corresponds to a byte value, which stores a greyscale value [0-255] that represents the attenuation of the rock at that point in space. This value is proportional to the density of the material: the higher the value, the denser is the system. Typically, the pore space has low attenuation values. The permeability and porosity of this particular sample of rock have not been measured. However, a permeability of 2 Darcy and a porosity of 22% are typical values for Bentheimer sandstones. Using this estimated rock porosity, it is

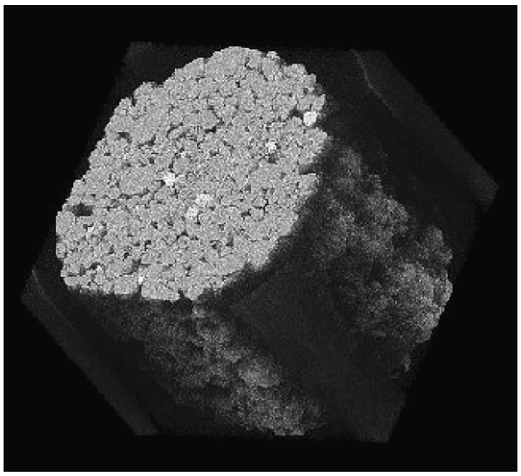

Fig. 6. 3D volume rendering of the XMT image of the Bentheimer sandstone used in this study.

possible to determine a threshold in the greyscale, to discriminate between pores and rock, and use this threshold to filter the attenuation values of the XMT image to generate a binary (0 pore site, 1 rock site) representation of the rock and the pore space. This representation can then be directly loaded into the lattice-Boltzmann code, and used as the rock matrix (solid boundary) for the simulations. We also define the void fraction ϕ in a rock sample as the number of "fluid" lattice points (*i.e.* the lattice points which are not on a solid obstacle) divided by the total number of lattice points. The void fraction is related to the porosity of the rock, which can be characterised experimentally by e.g. mercury porosimetry.

2.2. Results

2.2.1. Validation of Darcy's law

Calculations of single phase flow for different forcing values were performed and each simulation was run until the steady state was achieved (*i.e.* until the average flux was constant in time). The flux across each slice in the xy-plane (perpendicular to the direction of the flow) can be calculated according to

$$J(z) = \frac{1}{n_x\, n_y} \sum_{x,y=1}^{n_x,n_y} v(x, y, z), \quad z = 1, \ldots, n_z \tag{7}$$

where x, y and z denote the coordinates of a lattice site, and n_x, n_y and n_z are the system sizes (in lattice points). Because of mass conservation and fluid incompressibility, the flux in each longitudinal slice parallel to the main flow direction (z-axis) should be constant. However, small compressibility effects were observed in our lattice-Boltzmann simulations, resulting in a variation of the values of $J(z)$ with z, as shown in Fig. 7. The compressibility effects depend on the fluid velocity, and hence these differences increase with increasing flow driving force. To take into account these fluctuations, we calculate the average flux, $\bar{J}$ as

$$\bar{J} = \frac{1}{n_z} \sum_{z=1}^{n_z} J(z). \tag{8}$$

The average flux, $\bar{J}$, as a function of applied force, g, in a 128^3 lattice sites sample of the Bentheimer, shows linear behaviour (with zero intercept). This is predicted by Darcy's law for low forcing. The permeability can be calculated from the slope of the plotted line in the region where linear behaviour is observed. Once the right forcing regime is found, it is sufficient to compute the flux for one forcing level and the permeability can be directly calculated using expression (2). For all the simulations presented in this study we have chosen a value of the force $g = 0.0001$. The minimum number of steps required to reach steady state is, in general, system size dependent. Using $g = 0.0001$ as the driving force, and $\tau = 0.6$ as the BGK relaxation parameter, we have verified that 5000 steps are sufficient for equilibration, even in the largest sample (512^3) that we have considered in this work. For this number of steps, average quantities, such as flux, have reached equilibrium. Note, however, that the local densities and velocity fields are not yet fully equilibrated after 5000 steps, and it takes about 8000 steps for the microscopic quantities to reach steady state.

We find good agreement between the calculated values of the flux as a function of applied force and the linear behaviour predicted by Darcy's law. This is an example of how microscopic quantities, such as the velocity field at the pore scale computed using the lattice-Boltzmann method, can be related to macroscopic, phenomenological laws.

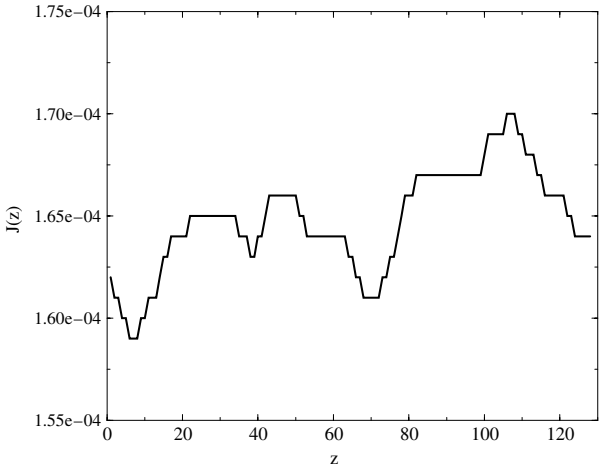

Fig. 7. Flux, $J(z)$, across each cross sectional area perpendicular to the forcing–and main flow–direction (z-axis) with body force $g = 0.0001$. The flux is expressed in lattice units.

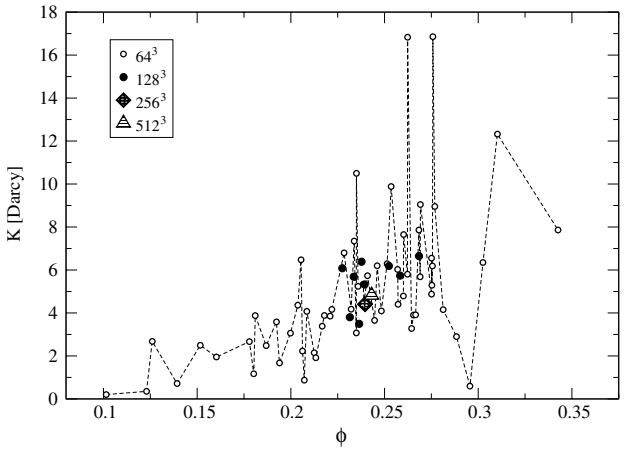

Fig. 8. Permeability, K (in Darcy) as a function of void fraction, ϕ, for rock samples of different size. The dotted line connecting the points for the systems of size 64^3 is only a guide to the eye.

We note that the measured permeability of porous media depends on the selected relaxation parameter in case of the BGK approach. This has been reported in the literature, e.g. by Pan et al. [20]. Also, we have reported on this dependence in a recent paper [10]. Here, we have chosen the relaxation parameter τ to be 0.6, corresponding with viscosity $\nu = 0.035$. We have shown that this value gives the smallest deviation between analytical and simulation results for the conductance in a rectangular capillary [10].

2.2.2. *Effect of system size*

In this section we show how the permeability of a realistic rock sample depends on the size of the sample, *i.e.* on the portion of rock used in the simulations to calculate the flux. The issue is addressed by considering samples of different sizes, and by studying the distribution of permeability as the sample size increases. The largest size we have considered is a 512^3 cube, centered in the middle of the full data set, then a 256^3 cube, also centered in the middle of the full data set. The 256^3 sample has then been divided into 8 and 64 cubes of size 128^3 and 64^3, respectively. To give an idea of the physical size of these samples, consider that a 64^3 cube has a linear size of 313 μm. The permeability has been computed in all these samples. The values of permeability, K, as a function of void fraction ϕ are reported in Fig. 8. Observe how the data for the smaller size we have considered (64^3) are more spread-out, both in ϕ and in permeability, while, as the system size increases, the data tend to concentrate into a narrower region. On the average, we found that, based on the 64^3 data, the permeability increases almost linearly with increasing void fraction, although for the smallest samples we observed large fluctuations.

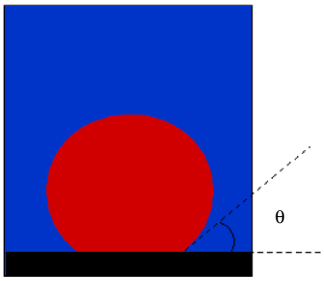

Fig. 9. Schematic illustration of how the contact angle θ is defined.

2.3. Phase separation

In this section, we present results of immiscible fluid flow modeled using the Shan–Chen model [21]. For more details, see [21,22]. We will first study phase separation and wettability effects. Then we will describe calculations of relative permeabilities in the Bentheimer rock sample.

The phase separation of a binary immiscible mixture depends on a number of parameters of which the most important is the value of the coupling constant $g_{\sigma\bar{\sigma}}$ between the two phases. Previous studies have shown that the surface tension increases linearly with increasing coupling constant [5]. Lattice-Boltzmann simulations of critical spinodal decomposition in binary immiscible fluids [23] were also carried out to determine the properties of a binary mixture as function of different parameter sets. Different wettabilities are implemented in our model by assigning to the solid sites (the surface) a virtual density of the wetting phase. For example, for water wettability, if the bulk density of the water phase is $\rho = 0.8$, then a virtual density between 0 (non-wet) and 0.8 (maximal wettability) can be assigned to the solid sites. Of course, this density is not evolving with the lattice-Boltzmann equation, but exerts a force on the neighboring fluid sites of the opposite phase, with the same coupling constant as the fluid–fluid interaction. The value of the wettability is given by the solid site density divided by the wetting fluid bulk density.

To verify that our implementation of two phase flow simulations with the lattice-Boltzmann method is able to model a wide range of wettability situations, we used a simple model of a box containing two immiscible fluids above a surface with variable wettability (see Fig. 10). The non-wetting fluid (oil, coloured in red) is initially placed in a cubic configuration at the center of the box and in contact with the surface, then a lattice-Boltzmann simulation is performed until the non-wetting phase has reached its equilibrium shape. The results are shown in Fig. 10 for oil concentration of 25%. When the surface is non-wet (wet $= 0$), the non-wetting phase spreads over the entire surface. As the wettability is increased, the non-wetting phase starts to detach from the surface, and forms a contact angle with it. This contact angle can be defined as the angle between the wet surface and a plane tangent to the non-wetting phase droplet where the droplet starts to detach from the surface, as illustrated in Fig. 9. This contact angle increases with increasing wettability. At large wettability (≥ 0.6) the non-wetting phase is completely detached from the surface and forms a spherical bubble.

2.4. Relative permeabilities

We carried out an extensive parameter study to find the optimal value of the total density that gives both phase separation and stability. Using this parameter, we calculate the relative permeabilities for both oil and water, forcing either oil or water or both. The initial condition for the distribution of fluids is a homogeneous saturation of the rock, where the saturation at each node is fixed. This means that, at each lattice site, the fractions of oil and water are fixed. In all cases, we run the simulations until a steady state is achieved. The results are shown in Fig. 11. In all cases, the rock is considered to be water-wet. We observe that the results for the non-wetting fluid (oil) do not depend on whether only the wetting phase is subject to a driving force or both phases are forced. For the case of the wetting fluid (water), on the other hand, the results depend on whether we force water or both water and oil. For more details, we refer to [22].

3. Conclusions

We have used lattice-Boltzmann simulations to calculate the flow in complex 3D porous media. First, we calculate the single phase permeability and detailed flow field for a 2D micromodel using an effective drag force to represent the third dimension. Our results are in good agreement with experiments. Tracer dispersion calculations were also carried out and predictions of the displacement propagator distributions were made. Second, we considered the flow in a realistic 3D rock sample of Bentheimer sandstone. We found that Darcy's law is valid in a wide range of forcing values, and that permeability values strongly depend on the size of the rock sample, showing a broad distribution for small samples. Finally, we have presented preliminary results on relative permeabilities in binary mixtures and we have shown that these permeabilities depend on the forcing conditions.

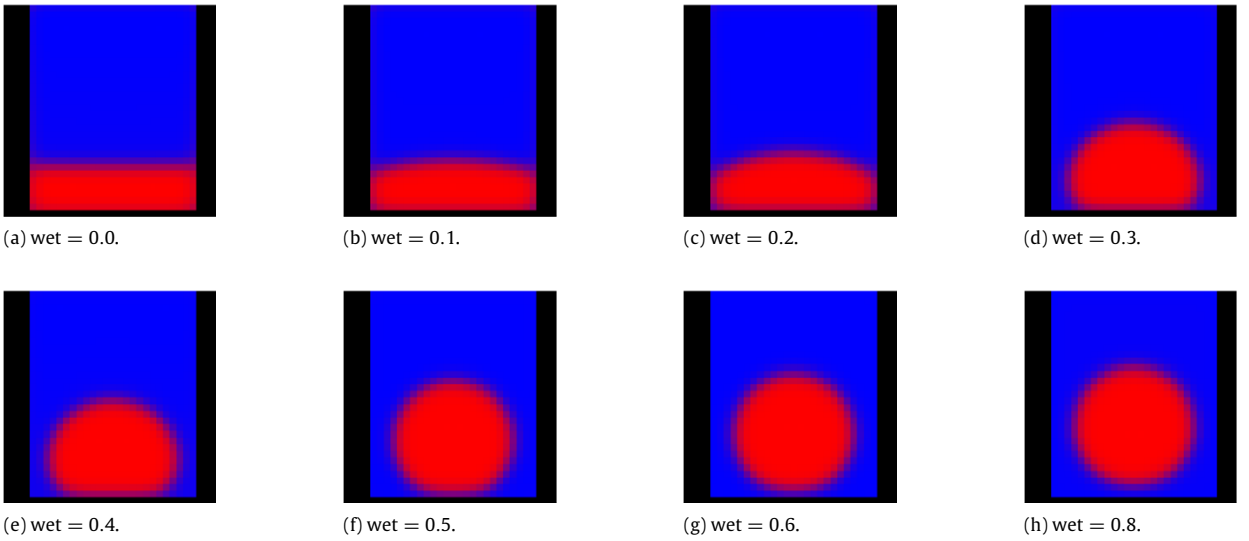

(a) wet = 0.0. (b) wet = 0.1. (c) wet = 0.2. (d) wet = 0.3.

(e) wet = 0.4. (f) wet = 0.5. (g) wet = 0.6. (h) wet = 0.8.

Fig. 10. Equilibrium configurations (as 2D slices taken at the center of the 3D system) of a binary immiscible fluid mixture as a function of increasing water wettability of the bottom surface. Wetting phase (water) is depicted in blue and non-wetting phase (oil) in red. Note the finite size effects in panels (b) and (c) where the detaching droplet of oil touches the lateral boundaries of the box. In this case, it is not possible to determine the contact angle. However, there are no finite size effects for all the other values of wettability. (For interpretation of the references to colour in this figure legend, the reader is referred to the web version of this article.)

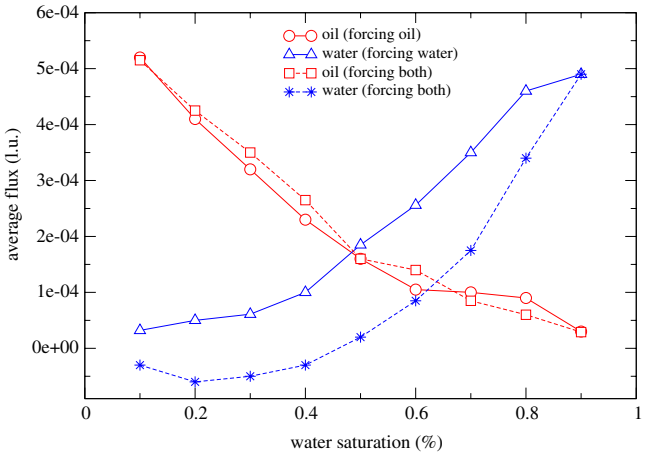

Fig. 11. Relative permeabilities in Bentheimer sandstone (sample size 128^3 lattice points).

Acknowledgments

We are grateful to Peter Coveney for facilitating this work and to Jonathan Chin, Silke Sheppard and John Crawshaw for helpful discussions. This research was partially supported by the EPSRC RealityGrid grants GR/R67699/01 and GR/R67699/02. To carry out the most computationally expensive simulations presented in this paper, resources on a Cray XT3 (“LeMieux”) at Pittsburgh PSC HPC facility (USA) were used.

References

[1] B. Ferrèol, D.H. Rothman, Lattice-Boltzmann simulations of flow through Fontainebleau sandstone, Transp. Porous Media 20 (1995) 3–20.
[2] A. Cancelliere, C. Chang, E. Foti, D. Rothman, S. Succi, The permeability of a random medium: Comparison of simulation with theory, Phys. Fluids A 2 (1990) 2085–2088.
[3] N.S. Martys, H. Chen, Simulation of multicomponent fluids in complex three-dimensional geometries by the lattice Boltzmann method, Phys. Rev. E 53 (1) (1996) 743–750.
[4] S. Succi, The Lattice Boltzmann Equation for Fluid Dynamics and Beyond, Oxford University Press, 2001.
[5] J. Chin, E.S. Boek, P.V. Coveney, Lattice Boltzmann simulation of the flow of binary immiscible fluids with different viscosities using the Shan-Chen microscopic interaction model, Proc. R. Soc. Lond. A 360 (2002) 547–558.
[6] E.S. Boek, J. Chin, P.V. Coveney, Lattice Boltzmann simulation of the flow of non-Newtonian fluids in porous media, Int. J. Mod. Phys. B 17 (2003) 99–102.

[7] S.P. Sullivan, L.F. Gladden, M.L. Johns, Simulation of power-law fluid flow through porous media using lattice Boltzmann techniques, J. Non-Newton. Fluid Mech. 133 (2006) 91–98.
[8] P. Grosfils, J.P. Boon, Viscous fingering in miscible, immiscible and reactive fluids, Int. J. Mod. Phys. B 17 (1–2) (2003) 15–20.
[9] P. Grosfils, J.P. Boon, J. Chin, E.S. Boek, Structural and dynamical characterization of Hele-Shaw viscous fingering, Proc. R. Soc. Lond. A 362 (2004) 1723–1734.
[10] M. Venturoli, E.S. Boek, Two-dimensional lattice-Boltzmann simulations of single phase flow in a pseudo two-dimensional micromodel, Physica A 362 (2006) 23–29.
[11] E.G. Flekkøy, U. Oxaal, J. Feder, T. Jøssang, Hydrodynamic dispersion at stagnation point: Simulations and experiments, Phys. Rev. E 52 (5) (1995) 4952–4962.
[12] E.S. Boek, M. Venturoli, Two-dimensional lattice-Boltzmann simulations of single phase flow in micromodels, in preparation (2009).
[13] C.L. Perrin, P.M.J. Tardy, K.S. Sorbie, J.P. Crawshaw, Micro-PIV: A new technology for pore scale flow characterization in micromodels, EAGE SPE Europe 2005, 94078 (2005) 933–940.
[14] B. Zerai, B.Z. Saylor, J.R. Kadambi, M.J. Oliver, A.R. Mazaheri, G. Ahmadi, G.S. Bromhal, D.H. Smith, Flow characterization through a network cell using particle image velocimetry, Transp. Porous Media 60 (2005) 159–181.
[15] S. Sirivithayapakorn, A.A. Keller, Transport of colloids in saturated porous media: A pore-scale observation of the size exclusion effect and colloid acceleration, Water Resour. Res. 39 (2003) WR001583.
[16] M. Auset, A.A. Keller, Pore-scale processes that control dispersion of colloids in saturated porous media, Water Resour. Res. 40 (2004) W03503.
[17] U.M. Scheven, D. Verganelakis, R. Harris, M.L. Johns, L.F. Gladden, Quantitative nuclear magnetic resonance measurements of preasymptotic dispersion in flow through porous media, Phys. Fluids 17 (2005) 117107.
[18] G. Picard, K. Frey, Method for modeling transport of particles in realistic porous networks: Application to the computation of NMR flow propagators, Phys. Rev. E 75 (2007) 066311.
[19] R.S. Maier, D.M. Kroll, R.S. Bernard, S.E. Howington, J.F. Peters, H.T. Davis, Pore-scale simulation of dispersion, Phys. Fluids 12 (8) (2000) 2065–2079.
[20] C. Pan, L.S. Luo, C.T. Miller, An evaluation of lattice Boltzmann schemes for porous medium flow simulation, Comput. Fluids 35 (2006) 898–909.
[21] X. Shan, H. Chen, Lattice Boltzmann model for simulating flows with multiple phases and components, Phys. Rev. E 47 (3) (1993) 1815–1819.
[22] E.S. Boek, M. Venturoli, Lattice-Boltzmann simulation of single phase and immiscible fluid flow in bentheimer sandstone, in preparation (2009).
[23] N. González-Segredo, M. Nekovee, P.V. Coveney, Three-dimensional lattice-Boltzmann simulations of critical spinodal decomposition in binary immiscible fluids, Phys. Rev. E 67 (2003) 046304.